energies

MDPI

Article

Biogenic Methane Accumulation and Production in the Jurassic Low-Rank Coal, Southwestern Ordos Basin

Chao Zheng [1,2], Dongmin Ma [1,3,*], Yue Chen [1], Yucheng Xia [1], Zheng Gao [4], Guofu Li [3] and Weibo Li [5]

[1] School of Geology and Environment, Xi'an University of Science and Technology, Xi'an 710054, China; zhengc0624@126.com (C.Z.); cyxust@126.com (Y.C.); xiayc823@163.com (Y.X.)
[2] School of Energy Engineering, Long Dong University, Qingyang 745000, China
[3] State Key Laboratory of Co-Mining Coal and Coalbed Methane Technology, Jincheng 048000, China; liguofu114@126.com
[4] School of Energy and Power Engineering, Xi'an Jiaotong University, Xi'an 710049, China; gaozheng@stu.xjtu.edu.cn
[5] Shaanxi Geological Science and Technology Center, Xi'an 710054, China; liweibo022@126.com
* Correspondence: mdm6757@126.com

Abstract: Geological conditions are the key for coalbed methane (CBM) accumulation and production. However, the geological feature of CBM accumulation and production in the Jurassic of Ordos Basin lacks systematic and detailed evaluation, resulting in poor CBM production in this area. This study has determined the genetic types of gas according to geochemistry characteristics of the gas, the geological factors to control CBM accumulation and production performance were revealed, and a comprehensive method was established to evaluate favorable areas based on 32 sets of CBM well production data from Jurassic Yan'an Formation. The results show the coal macerals are rich in inertinite (41.13~91.12%), and the maximum reflectance of vitrinite ($R_{o,max}$) in coal is 0.56~0.65%. According to gas compositions and carbon isotopes analysis, the $\delta^{13}C(CH_4)$ is less than −55‰, and the content of heavy hydrocarbon is less than 0.05%. The value of $C_1/(C_2 + C_3)$ is 6800~98,000, that is, the CBM is a typical biogenic gas of low-rank coal. The CBM accumulation model is the secondary biogenic on the gentle slope of the basin margin, in which gas content is closely related to buried depth and hydrodynamic environment, i.e., the high gas content areas are mainly located in the groundwater weak runoff zone at the burial depth of 450 m~650 m, especially in the syncline. Meanwhile, gas production mainly depends on the location of the structure. The high gas production areas of vertical wells were distributed on the gentle slope with high gas content between anticline and syncline, and the horizontal wells with good performance were located near the core of the syncline. According to the above analysis combined with the random forest model, the study area was divided into different production favorable areas, which will provide a scientific basis for the CBM production wells.

Keywords: low-rank coal; biogenic methane; geological factor; accumulation; production

Citation: Zheng, C.; Ma, D.; Chen, Y.; Xia, Y.; Gao, Z.; Li, G.; Li, W. Biogenic Methane Accumulation and Production in the Jurassic Low-Rank Coal, Southwestern Ordos Basin. *Energies* **2022**, *15*, 3255. https://doi.org/10.3390/en15093255

Academic Editors: Mofazzal Hossain, Shu Tao, Dengfeng Zhang, Huazhou Huang, Shuoliang Wang and Yanjun Meng

Received: 16 March 2022
Accepted: 26 April 2022
Published: 29 April 2022

1. Introduction

China is a large country of coal production and energy consumption, the large-scale and high-efficiency development of CBM can not only reduce mine gas accidents but also supplement the shortage of conventional natural gas [1,2]. Coalbed methane (CBM) is an important environment-friendly energy resource [3,4]. CBM includes biogenic gas and thermogenic gas, of which biogenic gas is generated dominantly by anaerobic bacteria and methanogens via coal biodegradation at low temperatures (<5 °C) [5–7]. Influenced by generation time and geological evolution, the biogas nowadays in coal reservoirs is secondary biogenic gas, which mainly is the reduction in carbon dioxide according to the gas component [8]. The resources of CBM are abundant in China, and commercial development for the middle-high rank CBM has achieved technological

breakthroughs [9–13]. Although the CBM resources of low-rank are rich [14,15], the development of low-rank CBM in western China is still not satisfactory [16–20].

Both scientific research and production practice show that it is a key step to making clear the geological characteristics of CBM accumulation and production. It was considered that CBM generation, accumulation and production are controlled by sedimentation, coalification, tectonism, hydrodynamics, as well as other geological factors [14,16,21–23]. The coalbed methane well productivity performance was a result of the strong interaction of cumulative thickness, burial depth, gas content, permeability, and reservoir pressure of fractured coal seam [24], in which the gas content is positively correlated with the coal burial depth, coal thickness [25]. The geologic structural setting and hydrogeological influenced the spatial distribution of gas content and permeability and so on [26–28]. Hydrodynamic confinement results in relatively high gas content of coal reservoir in the groundwater stagnation zone, while gas content is comparatively low in the recharge and runoff zones [11,29,30]. Characteristics of in situ stress indirectly control coalbed methane development by affecting permeability [31–33]. In a word, if the main controlling factors, such as structure, coal-forming environment, and hydrologic geology, are matched well, the enriched coalbed methane zone with high production would be formed [15].

Although much literature has been published on the geologic feature of CBM reservoirs [33–36], previous investigations on the CBM in the study area were mainly focused on geological background and CBM enrichment conditions [37–39]. Furthermore, the usual methods for the prediction of favorable areas are empirical methods, such as expert scoring method, fuzzy comprehensive evaluation method, etc., which have subjective human factors to a large extent [40,41]. Few studies on the model of coalbed methane accumulation and production based on the genetic type of coalbed methane have been conducted in this area. In particular, the detailed evaluation of low-rank coal biogas in western China. In this study, the random forest data training method was used to train and classify the sample data in order to comprehensively analyze the accumulation and production of CBM taking the Dafosi minefield, Binchang mining area as the study area. Firstly, we determine the gas compositions and the genetic types; secondly, we analyze the key factors affecting the CBM accumulation and production and then reveal the relationship between the gas content, gas production and geological conditions. Finally, the rank of factors is determined with grey correlation, and the favorable area for CBM development was predicted in the study area by using the random forest method.

2. Methodology

2.1. Data Acquisition and Processing

The coal samples in this paper were all collected from the No. 4 coal seam of the Middle Jurassic Yan'an Formation in the Dafosi minefield, Binchang mining area. The 10 coal samples were selected for the determination of maceral composition and the reflectance of vitrinite in coal according to the Chinese national standard GB/T 16773-2008, GB/T 8899-2013 and GB/T 6948-2008. The coal samples were ground to a particle size less than 1.0 mm air-dried base sample, made into pulverized coal slices, and then the samples were polished and carried out maceral composition determination. Meanwhile, the samples were repolished and dried in a drying oven at 30 °C~40 °C for 4 h before carrying out the reflectance of vitrinite in coal determination.

Carbon isotopic characteristics of CH_4 are important to the gas performance of coal reservoirs [42]. The gas samples came from the surface CBM wells, including multi-branch horizontal wells DFS-C02, DFS-05, DFS-06, DFS-09, and vertical wells DFS-C01, U-shaped well DFS-C03 and V-shaped well DFS-04. Wasson-7890A gas chromatograph was used for gas composition determination, and thermo MAT253 gas isotope mass spectrometer was employed in doing carbon isotope. Taking a certain volume of CBM sample with an airtight syringe and injecting it into the Trace GC ultra; the hydrocarbon components in the sample were separated by the meteorological chromatograph Trace GC ultra and converted into carbon dioxide in the oxidation unit GC combustion, and then the gas flow

entered the isotope mass spectrometer MAT253 IRMS for the determination of carbon isotope components. Gas compositions and carbon isotopes are based on GB/T 13610-2003 and SY/T 5238-2008. The basic information of the test sample is shown in Table 1.

Table 1. Basic information of test sample.

Gas Compositions Sample			Coal Maceral Compositions		
Sample ID	**Burial Depth**	**Sample Size**	**Sample ID**	**Burial Depth**	**Sample Size**
DFS-C01	435 m	10~20 mL	DFS-C01	435 m	0.18~0.25 mm
DFS-C02	610 m	10~20 mL	DFS-D48	554 m	0.18~0.25 mm
DFS-C03	540 m	10~20 mL	DFS-D62	568 m	0.18~0.25 mm
DFS-C04	510 m	10~20 mL	DFS-M85	615 m	0.18~0.25 mm
DFS-05	590 m	10~20 mL	DFS-05	590 m	0.18~0.25 mm
DFS-06	480 m	10~20 mL	DFS-U53	435 m	0.18~0.25 mm
DFS-09	535 m	10~20 mL	DFS-09	535 m	0.18~0.25 mm
/	/	/	DFS-128	500 m	0.18~0.25 mm
/	/	/	DFS-134	448 m	0.18~0.25 mm
/	/	/	DFS-122	585 m	0.18~0.25 mm

2.2. Data Interpretation

In order to analyze the main controlling factors affecting CBM productivity, the grey correlation analysis method is introduced to quantitatively determine the correlation degree between each influencing factor and productivity, so as to objectively evaluate the influence degree of each geological factor on coalbed methane well productivity [39,43]. Grey correlation calculation is mainly divided into two processes, (1) correlation coefficient calculation, (2) calculation of correlation degree [44]. Random forest was used for favorable area evaluation and prediction. Random forest takes decision trees as the basic model to generate a series of differentiated decision tree models by building different training data sets and different feature spaces [45–48]. The random forest was constructed based on classification and regression trees in this paper. In the process of establishing each classification and regression tree, the splitting process of each node is completed by calculating the "purity" of the sample after the split. The classification and regression tree employ the *gini* coefficient to measure this so-called "purity", i.e., random forest uses the *gini* index to split the tree to complete the decision. The smaller the *gini* coefficient, the higher the purity of the sample and the better the effect of tree division. Assuming that the sample set T contains k categories, the Gini coefficient of the sample set can be expressed as [49]:

$$gini(T) = 1 - \sum_{i=1}^{k} p_i^2 \quad (1)$$

where, p_i is the probability that T contains class i. If T is divided into two subsets T_1 and T_2, the divided *gini* coefficient can be expressed as:

$$gini(T_1, T_2) = \frac{|T_1|}{|T|} gini(T_1) + \frac{|T_2|}{|T|} gini(T_2) \quad (2)$$

where, $|*|$ represents the number of elements in the current sample set.

The selection of CBM development prospect evaluation indicators vary in different areas. For low-rank coal development areas, the gas generation potential, storage performance and preservation conditions of the coal reservoir should be chosen. Through the analysis of the drilling and experimental data of the CBM wells, the main factors influencing the development potential and productivity of CBM, including resource conditions (gas content, ash, net coal seam thickness) and occurrence conditions (structural location, roof thickness), development conditions (permeability, reservoir pressure, burial depth) were selected as evaluation indicators. There are few faults in this area, mainly folds. In

order to quantitatively study the influence of folds on the development of CBM, qualitative indicators (structural locations) are assigned and quantified separately. The flank is 0.8, the syncline is 1, and the anticline is 0.6.

In order to prevent the strong correlation between the factors, resulting in a decrease in the running rate of the evaluation model and over-fitting of the running results, the correlation between the factors needs to be tested. This paper adopts the Pearson correlation coefficient (*PCC*) to analyze the degree of correlation between the factors. The larger the value, the stronger the correlation of the factors. The calculation formula of the correlation coefficient between the evaluation factors is [50].

$$PCC = \frac{\sum_{i=1}^{n}(x_i - \overline{x})\sum_{j=1}^{n}(y_i - \overline{y})}{\sqrt{\sum_{i=1}^{n}(x_i - \overline{x})^2 \sum_{j=1}^{n}(y_i - \overline{y})^2}} \quad (3)$$

where, x_i, y_i is the variable values of X_i and Y_i, respectively, $\overline{x}$ and $\overline{y}$ are the average values of X_i and Y_i, respectively. When $0 \leq |PCC| \leq 0.4$, it indicates that the factor is irrelevant or weakly correlated. When $|PCC| > 0.6$, it indicates that the factor is strongly correlated.

3. Geology Setting and Analysis

3.1. Geology Condition

The Binchang mining area is located in the Miaobin depression area on the northern margin of the Weibei flexure belt in the southern Ordos Basin, the surface is covered by loess formation, and the occurrence of Cretaceous strata exposed in the valley is relatively gentle [51]. The deep Jurassic hidden structure is generally a monoclinic structure with N 60°~70° E in strike and NW~NNW in the dip. A set of broad and gentle folds are developed on it, from south to north, Binxian anticline, Lujia–Xiaolingtai anticline, Mengcun syncline, Qilipu–Xipo anticline in order. According to the borehole, no fault structure is found in the area. The overall structure is a monoclinic structure inclined from southeast to northwest inherited from the Triassic basement, the stratum dip is gentle, on average 3~5°. The stratigraphic division belongs to the Ordos areas, from bottom to top, it is the Hujiacun Formation of the Upper Triassic System (T_{3h}), the Fuxian Formation of the Lower Jurassic System (J_{1f}), the Middle Jurassic Yan'an Formation (J_{2y}), Zhiluo Formation (J_{2z}), Anding Formation (J_{2a}), Lower Cretaceous Yijun Formation (K_{1y}), Luohe Formation (K_{1l}), Huachi Formation (K_{1h}), Neogene and Quaternary strata, as shown in Figure 1.

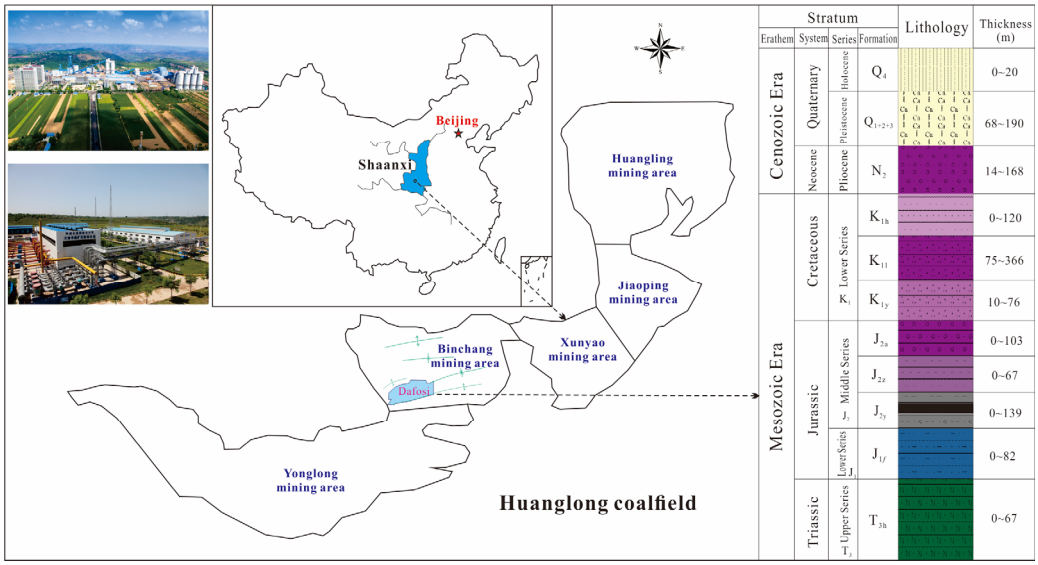

Figure 1. The location and stratum of Binchang mining area.

The overall structure of the study area is simple. As shown in Figure 2, the main structure is located on the southern flank of the Anhua syncline area to the north of the Binxian anticline. Due to the influence of synsedimentary structure, there are Anhua syncline, Qijia anticline, and Shijiadian syncline in order from north to south. The coal-bearing stratum in the study area is the Jurassic Middle Yan'an Formation, with a total of six coal-bearing seams, of which No. 4 coal is a relatively stable and main mineable coal seam in the minefield, distributed throughout the minefield. The stratigraphic occurrence and structural morphology show that the strata above Jurassic in this area have not been subjected to strong tectonic extrusion and deformation. The structure is closely related to the coal system, the deposition distribution of coal seams and their thickness changes. The coal seam is thicker at the syncline axis and thinner at the anticline axis. This pattern is mainly related to synsedimentary tectonics, and also reflects the inheritance of later tectonics.

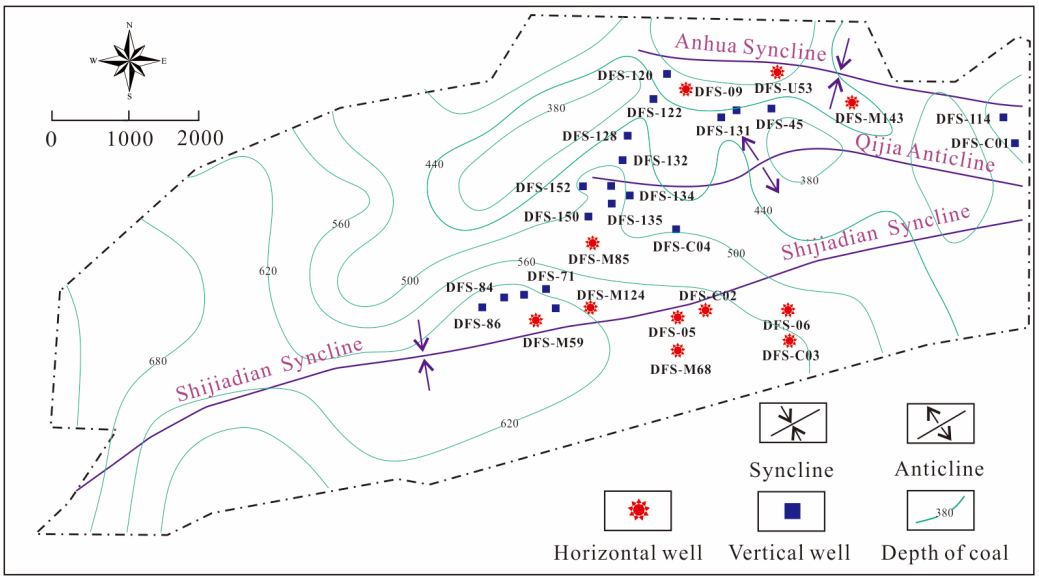

Figure 2. Structure characteristic of the study area.

CBM proved resources/reserves of the study area are 35.89 × 10^8 m^3, which are 25.5 × 10^8 m^3 in the No. 4 coal reservoir, and the average resource abundance is 1.44 × 10^8 m^3/km^2. CBM gas production capacity is 5.2 × 10^4 m^3/d, the average value of a single well can reach 1625 m^3/d. Consequently, the development potential of CBM is significant. The basic data used in this study, such as gas content and gas production, coal burial depth, thickness, lithology of overburden, etc., were collected from 32 CBM wells as shown in Table 2.

Table 2. Geological information of CBM well.

Well No.	Gas Production (m^3/d)	Gas Content (m^3/t)	Burial Depth (m)	Coal Thickness (m)	Permeability (mD)	Reservoir Pressure (MPa)	Ash of Coal (%)	Roof Thickness (m)
DFS-C02	11,270.97	4.30	610	11.00	7.70	2.80	14.00	2.20
DFS-05	10,600.96	2.80	590	16.80	10.00	3.30	11.00	2.10
DFS-M68	9625.14	3.60	589	14.00	9.20	3.10	12.00	2.00
DFS-M85	4025.73	8.10	615	11.80	6.60	3.20	15.50	2.10
DFS-09	3998.08	1.80	535	8.30	7.30	3.80	14.90	1.20
DFS-M143	3791.89	6.80	465	12.60	15.00	1.20	15.20	6.00
DFS-M124	3759.98	8.00	490	13.60	7.80	1.40	13.90	0.70
DFS-128	3256.75	3.30	500	10.30	3.80	2.90	10.50	0.70

Table 2. *Cont.*

Well No.	Gas Production (m^3/d)	Gas Content (m^3/t)	Burial Depth (m)	Coal Thickness (m)	Permeability (mD)	Reservoir Pressure (MPa)	Ash of Coal (%)	Roof Thickness (m)
DFS-C04	3145.28	8.30	510	12.20	11.00	5.50	15.90	3.00
DFS-148	2638.34	3.80	505	17.60	7.80	0.80	12.00	1.20
DFS-133	2590.39	8.00	490	10.20	6.80	4.30	17.00	0.60
DFS-CO1	2032.45	10.00	435	13.90	12.30	3.60	14.40	1.80
DFS-U53	1978.87	2.20	435	14.30	11.80	2.40	15.20	1.80
DFS-105	1936.58	7.70	500	8.30	7.40	5.50	15.80	1.40
DFS-45	1936.16	3.20	540	11.80	7.30	1.30	11.90	1.40
DFS-131	1876.32	2.80	570	10.20	4.80	2.50	19.00	1.50
DFS-134	1696.16	9.10	448	10.80	12.50	4.60	15.20	3.60
DFS-06	1339.94	8.30	480	11.00	18.80	5.60	15.10	6.80
DFS-C03	1248.76	3.50	540	12.30	6.00	6.00	16.00	0.80
DFS-132	836.56	8.20	505	8.30	7.40	6.00	15.20	1.40
DFS-122	683.15	8.60	585	20.30	6.50	3.30	17.00	2.60
DFS-114	579.37	9.30	630	13.50	8.00	3.80	16.80	3.00
DFS-152	554.33	8.10	510	12.30	8.10	4.80	16.30	1.00
DFS-M59	460.25	7.30	510	10.30	7.90	4.60	14.50	1.40
DFS-73	458.52	10.00	440	14.20	11.10	3.60	14.30	0.90
DFS-135	450.94	8.50	628	14.00	7.00	3.40	16.20	2.60
DFS-150	434.58	8.60	600	11.00	8.10	3.70	16.20	3.00
DFS-69	344.81	9.30	445	12.00	11.10	2.60	15.90	3.80
DFS-71	340.54	8.20	630	14.70	7.50	4.00	17.20	2.60
DFS-84	256.95	6.50	565	17.80	14.00	3.00	13.00	3.60
DFS-86	229.48	8.10	650	13.00	6.80	3.90	17.80	2.30
DFS-120	212.47	8.10	500	12.20	11.00	2.50	15.80	3.70

3.2. Geological Factors of Gas Content

3.2.1. Thickness of Coal Seam

Generally speaking, under the same conditions, the greater the thickness of the coal seam, the greater the amount of gas generated. The escape of gas is dominated by diffusion, and the concentration difference between two points in space is the main driving force for its diffusion [52]. The thickness of the No. 4 coal seam is 0.3 m~20.5 m in the study area, statistical analysis has indicated that the gas content is positively correlated with the thickness of the coal seam as shown in Figure 3a. The thicker the coal seam, the longer the gas diffusion path between the roof and floor, and the greater the diffusion resistance, which is more conducive to gas accumulation.

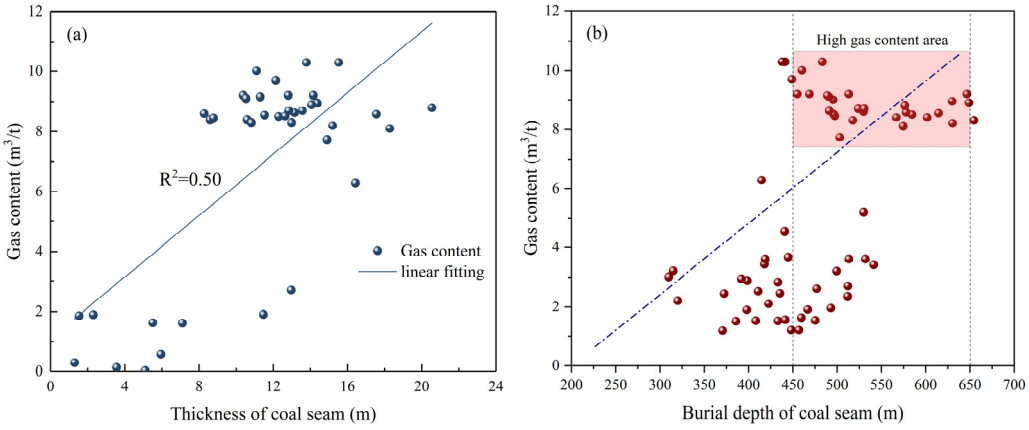

Figure 3. The relationship between gas content and thickness of coal seam, burial depth: (**a**) thickness of coal seam; (**b**) burial depth of coal seam.

3.2.2. Burial Depth and Structure

Burial depth is positively correlated with the reservoir pressure, and the larger reservoir pressure is conducive to the adsorption of gas. The migration distance of CBM to the surface with burial depth increases correspondingly, which is beneficial to the preservation of CBM. Therefore, the gas content generally increases with the increase in the burial depth of the coal seam. The burial depth of the No. 4 coal seam is 270 m~780 m from northeast to southwest. According to the analysis of the relationship between the burial depth and gas content, the area with gas content greater than 2 m^3/t is mainly distributed in 400 m~650 m as shown in Figure 3b, the gas content is low when the burial depth is less than 400 m. The main reason is that the shallow burial depth is in the groundwater recharge zone, and the overburden is thin, so the CBM is easy to escape. The groundwater stagnant zone with a buried depth exceeding 650 m is not conducive to the reproduction of methanogens, gas generation capacity itself is low. At present, the burial depth of coal seam with high gas content is mainly 450~650 m.

The structure of the study area is dominated by broad and gentle folds. Folds mainly affect the gas content by controlling the thickness of coal and the flow of groundwater, i.e., "syncline rich gas, anticline poor gas". There is a significant difference at different locations on the anticline and syncline. Above the neutral surface of the anticline axis, the coal seam and roof develop tensile fissures, and the gas is easy to escape. The groundwater flows from the axis of the anticline to the flanks, taking away part of the gas, which is not conducive to the accumulation of CBM. However, the coal rock above the neutral plane of the syncline is subjected to compressive stress, which is conducive to the preservation of gas with high gas content. It can be seen from Figure 4 that the content of the gas is more obviously controlled by structure style. The area with the highest gas content is the Shijiadian syncline axis area; the gas content of the Qijia anticline axis is relatively low.

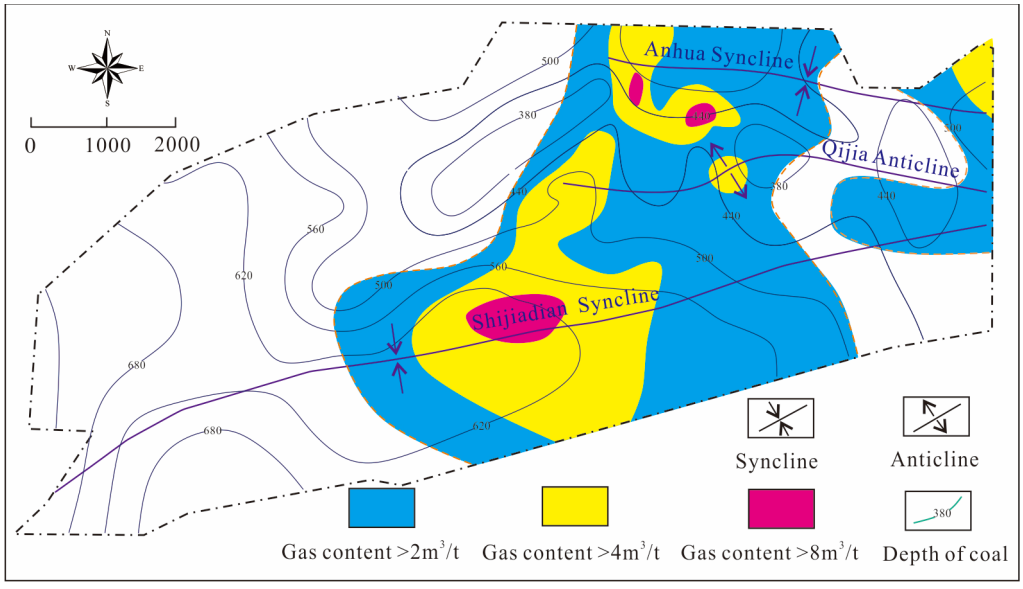

Figure 4. Geological structure and gas content distribution.

3.2.3. Hydrogeological Conditions

Hydrogeological conditions are an important factor affecting the occurrence of CBM [53,54], a positive relationship was found between gas content and basin hydrodynamics. As illustrated in Figure 5, it was found that the ions in the water of the Jurassic aquifer (Yan'an Formation and Zhiluo Formation) are mainly Cl^- and Na^+, the hydrochemical type is Cl^--Na^+, and the mineralization range is 13,781 mg/L~16,490 mg/L (Figure 6), which represents the water-bearing conditions of deepwater circulation and poor runoff, also provided favorable conditions for CBM accumulation. The main anions of the Cretaceous aquifers (Yijun Formation and Luohe Formation) are SO_4^{2-} and HCO_3^-,

the main cations are Na^+ and Mg^{2+}, and the hydrochemica types are SO_4^{2-}•Cl^--Na^+, SO_4^{2-}•(HCO^{3-})-Na^+•Mg^{2+}, the mineralization range are 859 mg/L~5790 mg/L. The hydrochemica type of the Xiaozhanggou Formation is HCO^{3-}-Na^+•Mg^{2+}•Ca^{2+}, and the mineralization is 274 mg/L~461 mg/L. The ions in the loose layer of the Quaternary system are HCO^{3-}, Na^+, Mg^{2+} mainly, the hydrochemical type is HCO^{3-}-Na^+•Mg^{2+}•Ca^{2+}, the water quality is good, and the mineralization is between 271 mg/L~317 mg/L (Figure 6). Low-rank coal located in the area of weak groundwater runoff, and low mineralization is conducive to secondary biogenic gas generation and hydrodynamic pressure-bearing sealing is conducive to the preservation of CBM.

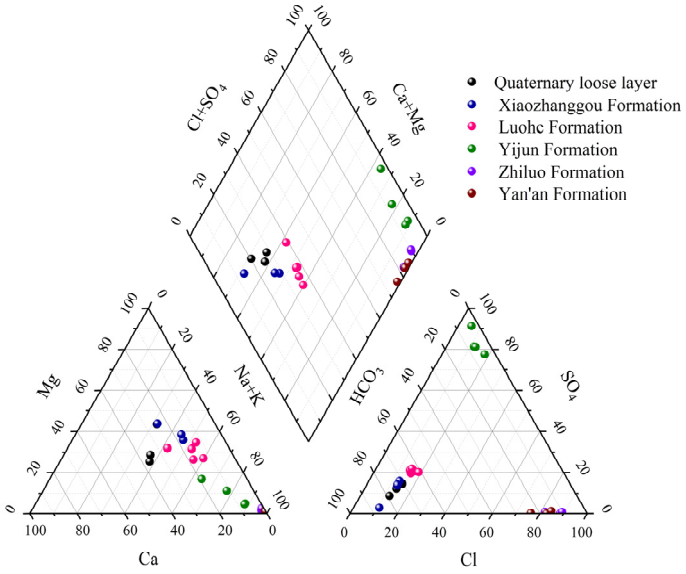

Figure 5. Hydrochemical type of groundwater.

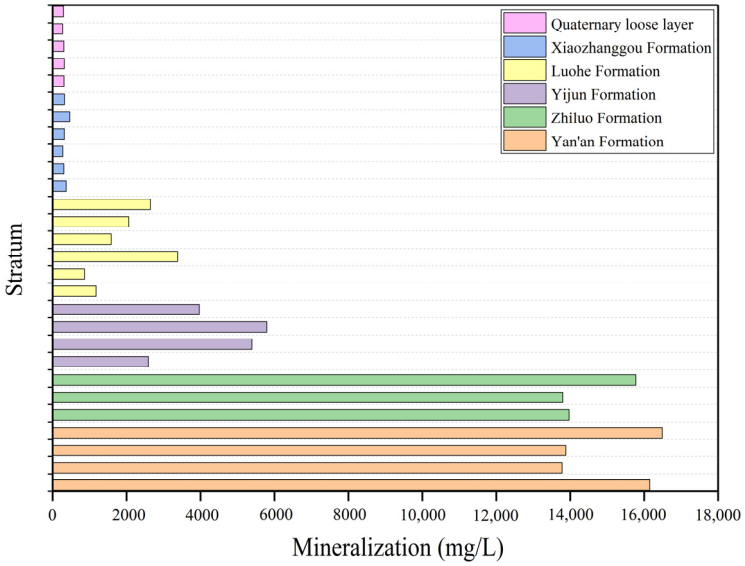

Figure 6. Mineralization degree of groundwater.

3.2.4. Lithology of Overburden Stratum

The lithology, thickness, development of joints and fissures of the roof above coal reservoirs are closely related to the accumulation of CBM. There are three mechanisms for the sealing effect of the roof on CBM, pressure and capillary can prevent gas migration, and hydrocarbon concentration mainly restrains gas diffusion [55]. The proper thickness and good sealing of the roof make the coal seam have the potential to preserve higher gas

content. The tighter the roof lithology is, the more beneficial it is for the accumulation of CBM. So, the greater the proportion of mudstone thickness in the Yan'an formation on the roof, the higher the gas content (Figure 7a). It is particularly emphasized that the thickness of mudstone within 10 m of the roof plays a more key role in the migration of CBM. As shown in Figure 7b, although the correlation between mudstone thickness within 10 m of the roof and gas content is not very significant if the immediate roof of the coal seam is mudstone, which is conducive to the accumulation of CBM.

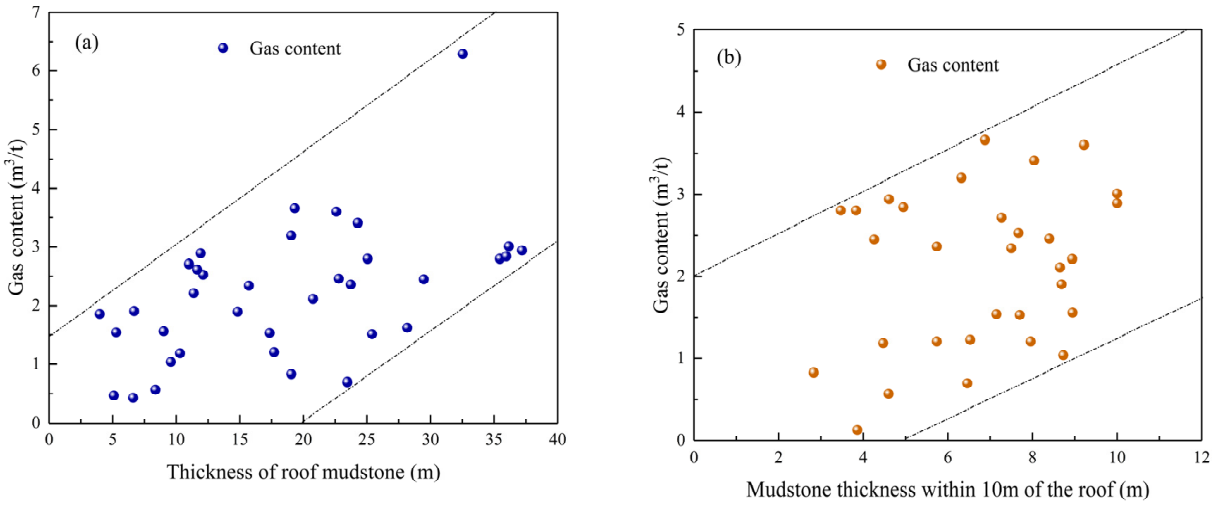

Figure 7. Relationship between gas content and roof: (**a**) mudstone thickness; (**b**) mudstone thickness within 10 m of the roof.

3.3. Geological Factors of Gas Production

3.3.1. Gas-Bearing Properties of Coal Reservoir

Gas content is a basic indicator of CBM storage performance and sufficient condition in the evaluation of CBM development prospects. Areas with high gas content are often favorable areas for CBM development. The gas content is mainly concentrated in 2 m^3/t~10 m^3/t, the gas production fluctuates in a wide range during the stable production stage (Figure 8).

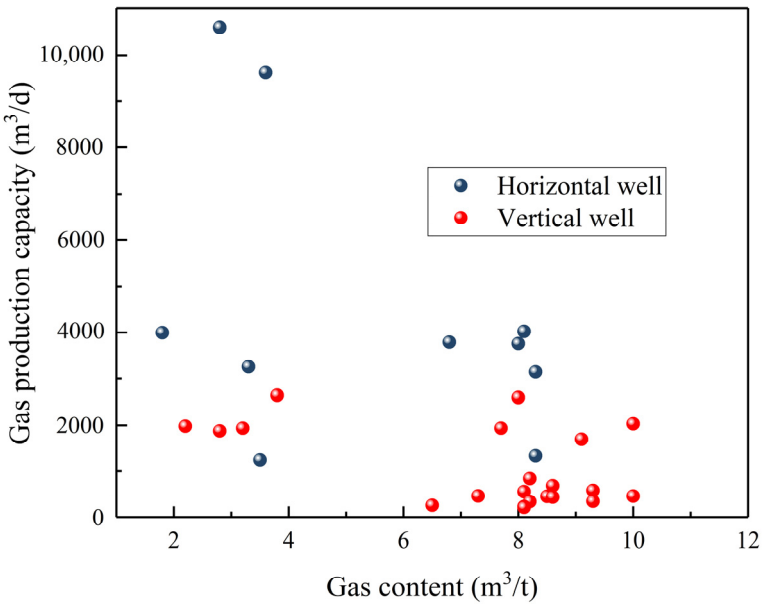

Figure 8. The relationship between gas production and gas content.

3.3.2. Burial Depth and Thickness of Coal Seam

The burial depth of coal seams directly affects coal seam permeability, in situ stress, and reservoir pressure. The burial depth of coal seams is between 400 m~650 m. It can be seen from Figure 9a that when the depth is greater than 550 m, the tendency of gas production to decrease with the increase in burial depth becomes more obvious. The thickness reflects the abundance of resources to a certain extent. The greater the thickness, the higher the resource abundance, and the gas production also increases. There is a positive correlation between the gas production and the thickness of the coal seam, especially with horizontal wells as shown in Figure 9b.

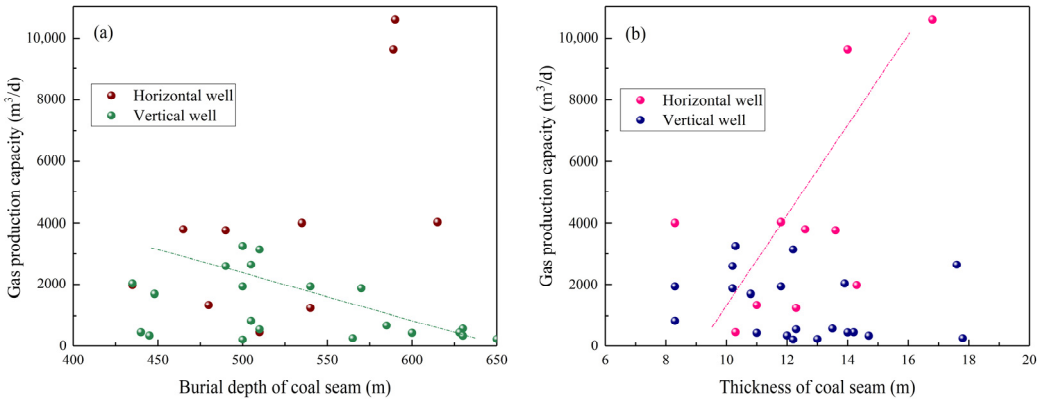

Figure 9. The relationship between gas production and burial depth, thickness of coal seam: (**a**) burial depth of coal seam; (**b**) thickness of coal seam.

3.3.3. Permeability and Reservoir Pressure

Permeability and reservoir pressure play an important role in the development of CBM and restrict the desorption and migration of CBM. According to field data, the permeability of the No. 4 coal reservoir is 2 mD~20 mD, the reservoir pressure is 2 MPa~8 MPa, and the gas production has no obvious correlation with permeability and reservoir pressure (Figure 10).

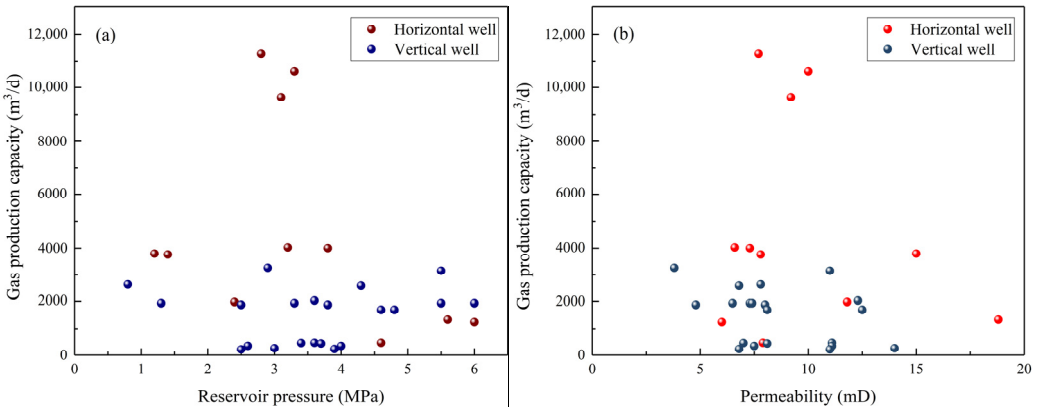

Figure 10. The relationship between gas production and reservoir pressure, permeability: (**a**) reservoir pressure; (**b**) permeability.

3.3.4. Structure Conditions

It was found that the fractures in the fold flanks are moderately developed, and the permeability of coal reservoirs as well. In the process of gas production, although it receives recharge from the anticline, underground water flows to the syncline core to make it easier for depressurization and gas migration. Therefore, the gas content of the fold flank and the permeability of the coal reservoir reach a suitable match, and the stable gas production of the CBM well is generally better. The Anhua syncline, Qijia anticline and Shijiadian syncline are developed in the study area. As shown in Figure 11, the gas production is closely related

to the structure position, but the difference between different well types is obvious. The vertical wells DFS-128 and DFS-C04 are located in the gentle slope between the fold flanks, which average gas production were 3256.75 m^3/d and 3145.28 m^3/d, respectively, in the stable production stage. However, the gas production of vertical wells was poor near the syncline axis. Horizontal wells DFS-C02, DFS-M124, and DFS-05 are located near the Shijiadian syncline axis. The average gas production in the stable production stage is about 11,270.97 m^3/d, 3759.98 m^3/d, and 10,600.96 m^3/d. Therefore, it can be summarized that the high production area of horizontal wells is between the syncline core and the vertical wells are between the fold flanks.

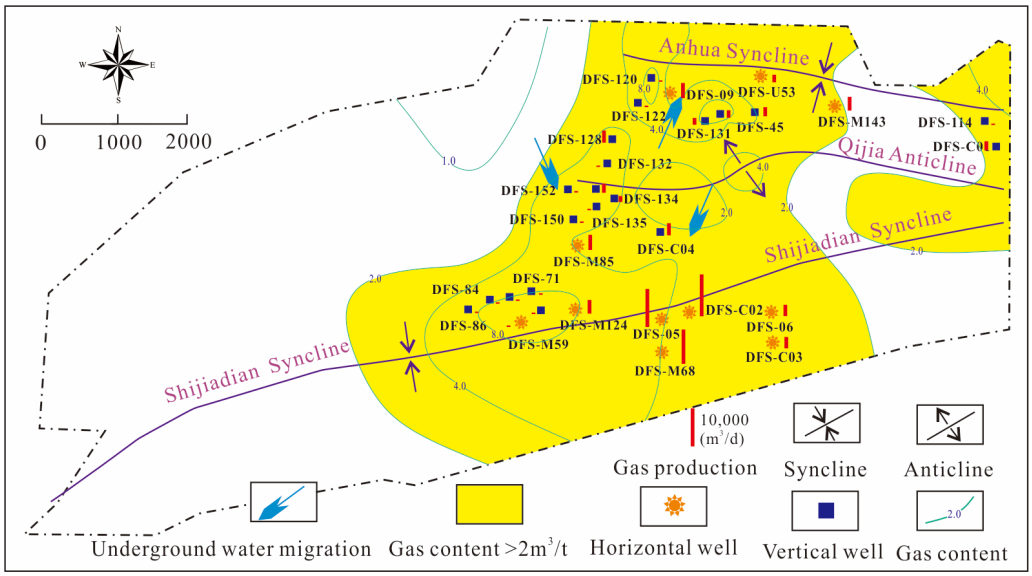

Figure 11. The relationship between gas production and structure.

4. Results and Discussion

4.1. Coal Sample Characteristics

The maximum vitrinite reflectance ($R_{o,max}$) of the coals is 0.56~0.65%. The coal macerals are mainly inertinite (41.13~91.12%), followed by vitrinite (6.93~49.3%), and the content of liptinite is the lowest (<9.52%) as shown in Table 3. Statistical analysis of the data found that the vitrinite is positively correlated with the gas content, and the fitting result R^2 value is 0.73, while the inertinite is negatively correlated (Figure 12), which is also consistent with the results of previous studies [51].

Table 3. Maceral of coal sample.

Sample ID	$R_{o,max}$/%	Maceral Compositions/%		
		Vitrinite	Inertinite	Liptinite
DFS-D48	0.58	6.93	92.12	0.95
DFS-D62	0.56	16.65	82.32	1.03
DFS-M85	0.65	18.94	77.84	3.22
DFS-09	0.59	20.17	74.55	5.28
DFS-U53	0.61	20.83	76.41	2.76
DFS-05	0.63	22.14	74.33	3.53
DFS-128	0.58	25.29	72.54	2.17
DFS-134	0.62	27.46	70.89	1.65
DFS-122	0.57	29.09	68.15	2.76
DFS-C01	0.63	49.30	41.18	9.52

Note: $R_{o,max}$ is maximum vitrinite reflectance of coal.

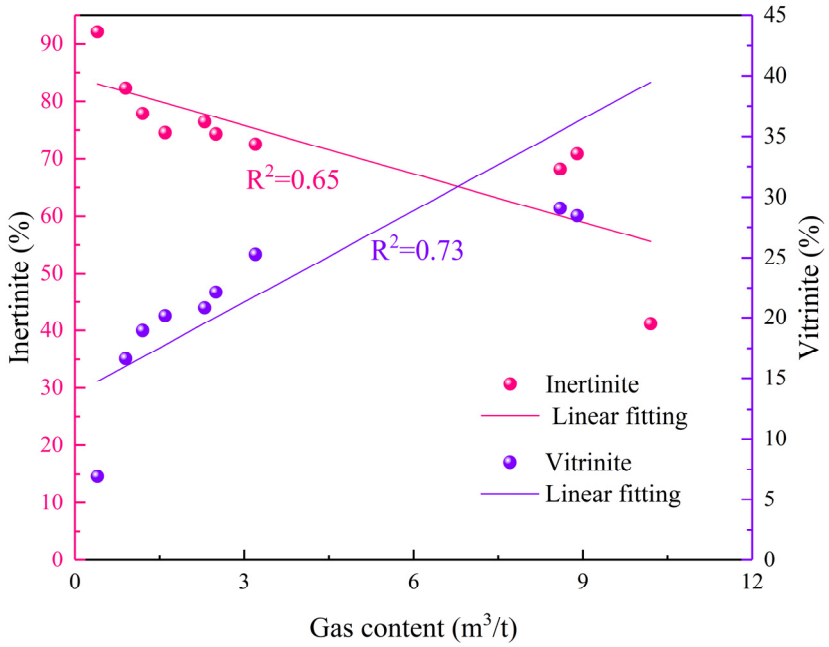

Figure 12. Correlation between gas content and macerals.

4.2. Geochemistry Characteristic of the Gas

The gas compositions (Table 4) show that the gas compositions include CH_4, CO_2, N_2, a small amount of O_2 and a trace of C_2H_6. The content of CH_4 is 68.35~97.95%, and C_2H_6 is 0.001~0.028%. The geochemical characteristics of carbon isotope determined that the $C_1/(C_2 + C_3)$ are 6800~98,000. The dry and wet index C_1/C_{1-5} of the hydrocarbon composition is 0.99991. The non-hydrocarbon compositions are mainly N_2, the content is 1.256~29.75%, and the content of CO_2 is 0.24~2.375%, with an average of 1.16%. The results of the isotope test showed that the $\delta^{13}C(CH_4)$ was −87.2~−68.9‰, with an average of −78.75‰, and the $\delta^{13}C(CO_2)$ was between −41.693‰ and −7.0650‰, with an average of −20.43‰.

Table 4. Gas compositions and carbon isotopes analysis.

Well No.	Initial Compositions						Stable Isotopes ‰	
	CH_4%	C_2H_6%	O_2%	N_2%	CO_2%	$C_1/C_2 + C_3$	$\delta^{13}CH_4$	$\delta^{13}CO_2$
DFS-C01	97.95	0.001	0.052	1.256	0.736	97,954.8	−80.52	−24.427
DFS-C02	89.25	0.009	0.267	8.785	1.684	9917.26	−77.25	−12.623
DFS-C03	88.84	0.01	0.273	9.684	1.198	7724.68	−78.88	−7.524
DFS-C04	91.58	0.009	0.211	5.825	2.375	10,175.57	−78.06	−41.693
DFS-05	78.7	0.028	0.4	19.47	1.32	7870	−76.50	−14.8
DFS-06	88.01	0.007	0.331	10.73	0.918	12,573.24	−75.21	−7.065
DFS-09	76.33	0.001	0.22	23.03	0.24	92,940.6	−73.78	−11.419
DFS-45	70.33	-	0.25	28.68	0.44	7033	−76.1	-
DFS-M68	77.88	-	0.24	21.12	0.65	7788	−68.9	−13.2
DFS-69	78.36	-	0.23	20.53	0.78	7836	−82.3	−20.3
DFS-128	84.32	-	0.12	13.49	2.01	8432	−83.7	−22.7
DFS-131	77.34	-	0.18	21.97	0.31	7734	−77.6	-
DFS-133	85.35	-	0.16	12.09	2.34	8535	−87.2	−36.6
DFS-148	68.35	-	0.39	29.75	1.3	6835	−86.5	−32.9

Note: DFS-45, DFS-M68, DFS-69, DFS-128, DFS-131, DF-133, DFS-148 [56].

The $\delta^{13}C_1$ is less than −55‰, and the content of heavy hydrocarbon is less than 0.05%. By comparing $\delta^{13}CH_4$ with $C_1/(C_2 + C_3)$, and the methane-genesis identification chart [57], it can be determined that the gas is a biogenic gas (Figure 13). The N_2 is 1.256~29.75%, with

an average of 16.17%. There is an obvious linear negative correlation between the content of N_2 and CH_4 (Figure 14), indicating that the coal seam was exposed to the surface or connected with surface water, N_2 in the atmosphere seeped into the coal seam with the water flow, resulting in the high N_2 content. The CO_2 content is 0.24~2.375% and the value of $\delta^{13}C$ (CO_2) is between −36.693‰ and −7.0650‰, it belongs to CO_2 of organic origin.

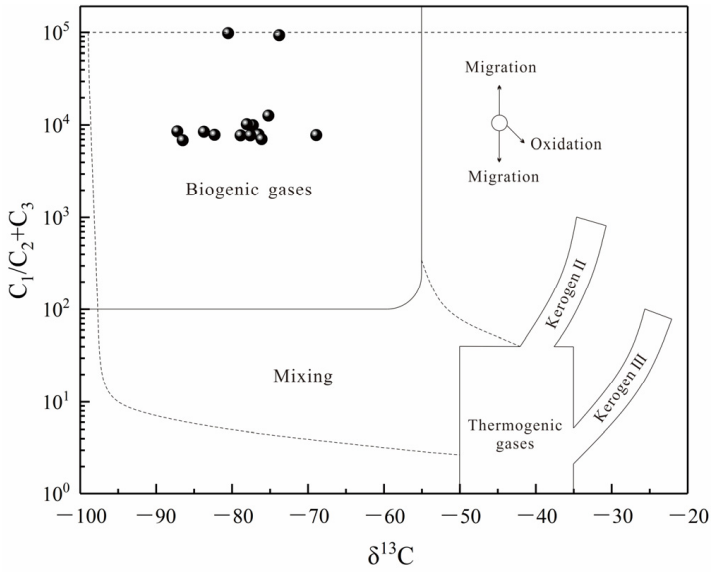

Figure 13. Identification chart of the genetic of CBM.

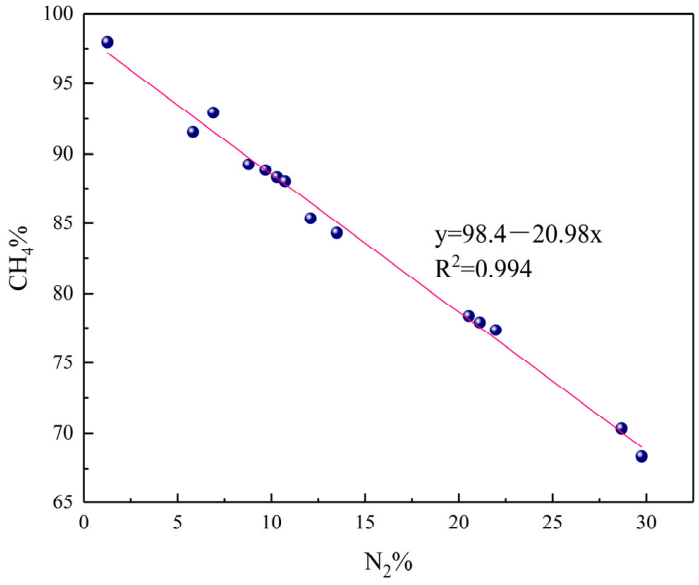

Figure 14. Correlation between N_2 and CH_4 in gas compositions.

The maximum vitrinite reflectance ($R_{o,max}$) has indicated that the coal of the study area was a low metamorphism degree. The coal seam was at the end of the primary biogenic gas and has not yet entered the thermal genetic stage of massive methane generation, which provided favorable material conditions for the generation of secondary biogenic gas. Based on the above comprehensive analysis, CBM was the typical secondary biogenic gas.

4.3. Geological Model of CBM Accumulation

In the geological evolution process of coal reservoirs, tectonic evolution plays a key role in gas generation through stratum subsidence and thermal evolution. Wang et al. [58] proposed the feature of the later tectonic of the Ordos coal-forming basin is the symbiosis

of the western thrust, the southern uplift and the fault depression. Near south-north thrust nappe structures developed in the western margin of the basin, leading to exposure and large-scale denudation of the Jurassic coal-bearing rock series. The study area is a northeast inclined monoclinic structure, the coal seam belongs to the Jurassic coal seam with shallow burial depth and low metamorphism degree ($R_{o,max}$ < 0.65%). When the coal seam was raised to the shallow area, the stratum fissure developed and atmospheric precipitation and surface runoff directly recharged the coal reservoir, which provided suitable geological environmental conditions for the reproduction of bacteria. Under the action of the methane bacteria, the organic matter turned into methane under physical and chemical. It was found that the relatively enriched area of CBM was mainly concentrated in the weak runoff zone of the basin margin slope with a burial depth of 450 m~650 m. The weak runoff zone has weak groundwater activity, which is conducive to the preservation of CBM reservoirs. The deep stagnant zone (>650 m) is insufficient to recharge the coal seams and the water mineralization is high, which is not conducive to the reproduction of methane bacteria and gas generation. According to the analysis results of 4.1 and 4.2, CBM was the secondary biogenic gas of low-rank coal. Based on the above comprehensive analysis, the CBM accumulation model is the secondary biogenic gas accumulation on the gentle slope of the basin margin (Figure 15).

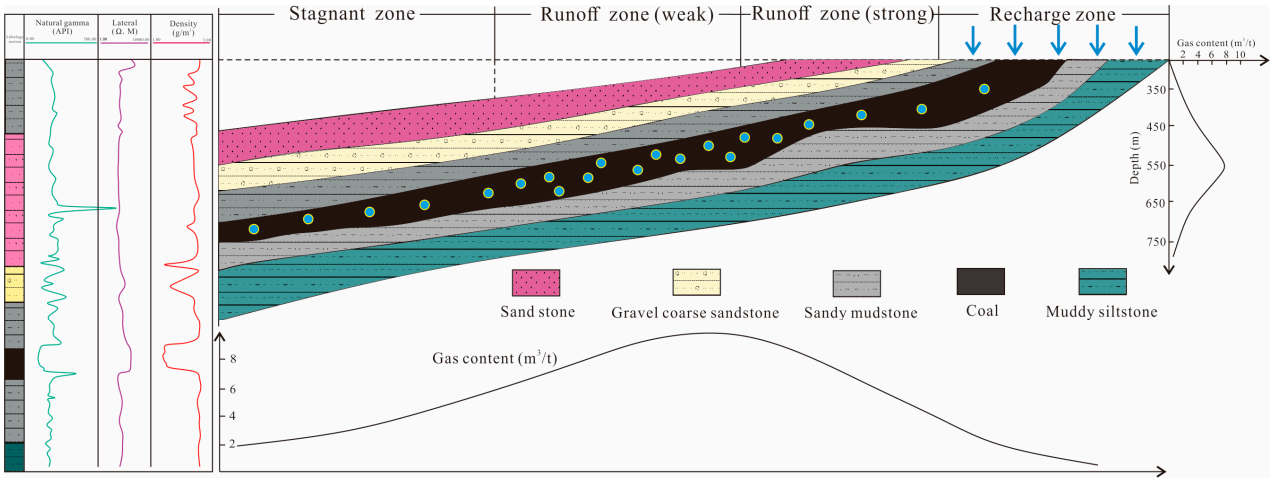

Figure 15. Geological model of CBM accumulation and enrichment.

4.4. CBM Production Analysis

4.4.1. Geological Factors Evaluation of CBM Production

As mentioned before, the main controlling factors of CBM production capacity include gas content, burial depth, coal thickness, structural, hydrological conditions, permeability, and reservoir pressure. Daily gas production is a key indicator reflecting production capacity, the average daily gas production at the stable production stage is considered as the dependent variable and other related factors as independent variables. The main control factors of gas production capacity were analyzed by the gray correlation. The calculation process of correlation degree refers to the literature [44,59,60]. The lithology of the No. 4 coal seam roof is all sandy mudstone or carbonaceous mudstone, and the difference in lithology is small. Therefore, the factors that can affect the CBM production capacity (gas production) include coal thickness, permeability, gas content, reservoir pressure, ash, roof thickness and burial depth. According to the results of the correlation degree, it can be seen that the main control factors of the productivity between vertical wells and horizontal wells are quite different, as shown in Table 5.

Table 5. Grey correlation quantitative evaluation of controlling factors of CBM production.

Vertical Well			Horizontal Well		
Factors	**Correlation**	**Rank**	**Factors**	**Correlation**	**Rank**
Coal thickness	0.662	1	Gas content	0.656	1
Burial depth	0.572	2	Coal thickness	0.622	2
Permeability	0.541	3	Reservoir pressure	0.579	3
Ash of coal	0.493	4	Ash of coal	0.579	4
Roof thickness	0.415	5	Permeability	0.555	5
Gas content	0.404	6	Roof thickness	0.427	6
Reservoir pressure	0.196	7	Burial depth	0.394	7

4.4.2. High Production Model of CBM

The study area as a whole is a monoclinic structure dipping from northeast to southwest. Except for DFS114 and DFS-C01 located in the eastern part of the minefield, the rests were distributed in the central area of the minefield. In terms of gas production, there are 19 production wells above 1000 m^3/d, in which horizontal wells DFS-C02 and DFS-05 have gas production rates of more than 10,000 m^3/d. High production vertical wells (>3000 m^3/d) include DFS-128 and DFS -C04.

Through the connected well profile of the high production well in the Dafosi minefield, DFS-128(V)—DFS-C04(V)—DFS-C02/-05(H)—DFS-M168(H) showed that the vertical wells DFS-128 and DFS-C04 were mainly distributed on the flanks of the anticline, while horizontal wells DFS-C02, DFS-05 and DFS-M168 were located near the core of the Shijiadian syncline, and the gas content of the high production wells are basically more than 4 m^3/t (Figure 16). The well positions of different well types have obvious differences, the high production area of vertical wells is located at the folding flank, and horizontal wells are located at the syncline axis. The roof mudstone and weak underground water sealing effect are conducive to forming the high gas content in the fold flank. Under the action of tensile stress, the fractures above the neutral of the fold are more developed and the permeability is good, which is conducive to rapid depressurization of the reservoir and gas production by drainage, e.g., the gas production of well DFS-128 during the stable production period is more than 3200 m^3/d. The thickness (12 m~20 m) and burial depth (500 m~600 m) of the coal seam at the syncline axis of Shijiadian are large. The hydrodynamic environment is a weak runoff zone. Due to the long horizontal section of the horizontal well, the influencing range in the coal seam is relatively wide. Good drainage and depressurization effect, high gas production, e.g., the gas production of DFS-C02 well during steady production period is about 11,000 m^3/d. Of course, apart from geological factors, drilling and production technologies, fracturing technologies and drainage systems all have a significant impact on gas production, but we will not discuss them here.

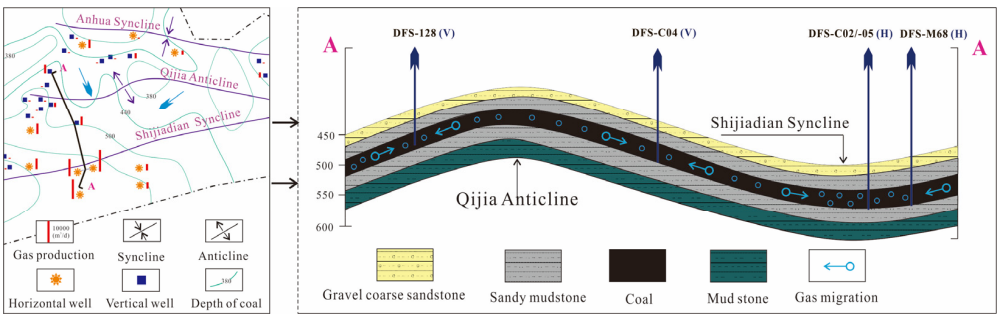

Figure 16. High-production model of CBM.

4.4.3. The Favorable Areas for CBM High Production

It can be seen in Table 6, that the absolute value of the correlation coefficient between all factors was less than 0.4, and the correlation coefficient of the structure position was also

close to 0.4. Therefore, the factors can be considered independent of each other. The gas production of CBM wells is quite different, the classification standard of high production and low production is the daily gas production in the stable production stage. If it is higher than 1500 m^3/d, it is regarded as high production, less than 1500 m^3/d is the low production. The attribute data of 12 high production wells and the same number of non-high production wells are randomly selected as the training sample set, and the remaining five high production wells and the rest of the non-high production well points form a test sample set. Based on MATLAB, the random forest model training sample set is used for learning, and the learned model is used in the test sample. The prediction rate of the model is 70%. Therefore, the model is considered reliable and can be used to evaluate the whole area in the next step.

Table 6. Correlation coefficient of main controlling factor.

Controling Factors	Gas Content	Burial Depth	Coal Thickness	Permeability	Reservoir Pressure	Structural Location	Ash of Coal	Roof Thickness
Gas content	1							
Burial depth	−0.130	1						
Coal thickness	0.044	0.186	1					
Permeability	0.284	−0.475	0.166	1				
Reservoir pressure	0.312	0.011	−0.396	0.021	1			
Structure location	0.417	0.199	−0.198	−0.122	0.350	1		
Ash of coal	0.194	−0.127	0.141	0.218	0.231	0.075	1	
Roof thickness	0.318	−0.047	0.106	0.768	−0.012	0.146	0.271	1

Subsequently, the attribute database of the study area was brought into the trained model, and the susceptibility index of high production CBM wells based on the random forest model was obtained, and the interval is [0, 0.948]. The natural discontinuity method was used to classify its susceptibility levels into three categories, which are the unfavorable area [0.03, 0.386], generally the favorable area [0.386, 0.51], and the extremely favorable area [0.51, 0.948], the predicted result of the generated favorable area of CBM is shown in Figure 17.

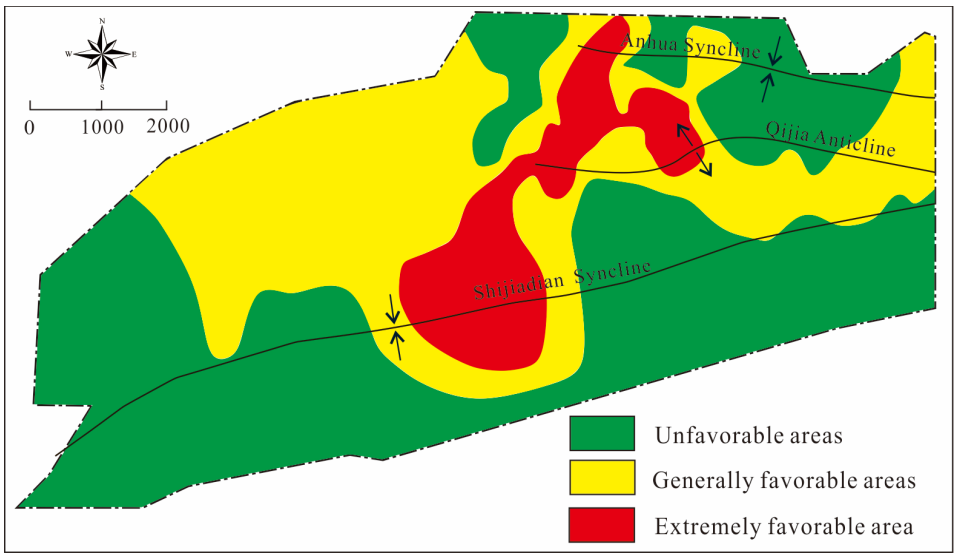

Figure 17. Prediction results of favorable areas in the study area.

5. Conclusions

(1) The maximum reflectance of vitrinite ($R_{o,max}$) in coal are 0.56~0.65%. The result of gas compositions and carbon isotopes analysis shows that CBM is typical biogenic gas of low-rank coal.

(2) The gas content is closely related to buried depth and hydrodynamic environment, i.e., the high gas content areas are mainly located in the groundwater weak runoff zone at the burial depth of 450 m~650 m, especially in the syncline. The CBM accumulation model is the secondary biogenic on the gentle slope of the basin margin.

(3) The productivity of CBM wells is closely related to the structural location, but vertical wells gas production performance is different from horizontal wells. The high gas production area of vertical wells is distributed on the gentle slope with high gas content between anticline and syncline, the horizontal wells with good performance are located near the core of the syncline.

(4) According to the random forest model, the study area is divided into three areas, which are the unfavorable area, the generally favorable area, and the extremely favorable area. The predicted results will provide the scientific basis for the CBM production wells.

(5) The CBM development of low-rank coal in Western China is still in the early stage. The study area is relatively small, and the number of samples is few. It is suggested that future research should be based on more production data. In addition, mining technology is an indispensable aspect of the research on CBM development, and the evaluation of geological factors should be combined with mining technology.

Author Contributions: Conceptualization, C.Z. and D.M.; methodology, Y.X.; formal analysis, Z.G.; investigation, C.Z.; data curation, W.L.; supervision, Y.X.; project administration, G.L.; funding acquisition, D.M. and Y.C.; writing—original draft preparation, C.Z.; writing—review and editing, D.M. All authors have read and agreed to the published version of the manuscript.

Funding: This work is supported by National Natural Science Foundation of China (Grant No. 41902175), the Shanxi Province Science and Technology Major Special Funding Project (Grant No. 20201101002).

Conflicts of Interest: The authors declare no conflict of interest.

References

1. Li, Y.; Wang, Z.; Tang, S.; Elsworth, D. Re-evaluating adsorbed and free methane content in coal and its ad- and desorption processes analysis. *Chem. Eng. J.* **2022**, *428*, 131946. [CrossRef]
2. Li, Y.; Yang, J.; Pan, Z.; Meng, S.; Wang, K.; Niu, X. Unconventional Natural Gas Accumulations in Stacked Deposits: A Discussion of Upper Paleozoic Coal-Bearing Strata in the East Margin of the Ordos Basin, China. *Acta Geol. Sin.-Engl. Ed.* **2019**, *93*, 111–129. [CrossRef]
3. Moore, T.A. Coalbed methane: A review. *Int. J. Coal Geol.* **2012**, *101*, 36–81. [CrossRef]
4. Mastalerz, M.; Drobniak, A. Coalbed Methane: Reserves, Production, and Future Outlook. In *Future Energy*; Elsevier: Amsterdam, The Netherlands, 2020; pp. 97–109. [CrossRef]
5. Guo, H.; Zhang, J.; Han, Q.; Huang, Z.; Urynowicz, M.A.; Wang, F. Important Role of Fungi in the Production of Secondary Biogenic Coalbed Methane in China's Southern Qinshui Basin. *Energy Fuels* **2017**, *31*, 7197–7207. [CrossRef]
6. Stolper, D.A.; Lawson, M.; Davis, C.L.; Ferreira, A.A.; Santos Neto, E.V.; Ellis, G.S.; Lewan, M.D.; Martini, A.M.; Tang, Y.; Schoell, M.; et al. Gas formation. Formation temperatures of thermogenic and biogenic methane. *Science* **2014**, *344*, 1500–1503. [CrossRef] [PubMed]
7. Li, Y.; Tang, D.; Fang, Y.; Xu, H.; Meng, Y. Distribution of stable carbon isotope in coalbed methane from the east margin of Ordos Basin. *Sci. China Earth Sci.* **2014**, *57*, 1741–1748. [CrossRef]
8. Whitiar, M.J.; Faber, E.; Schole, M. Biogenic methane formation in marine and freshwater environments: CO_2 reduction VS. acetate fermentation-Isotope evidence. *Gmchrm. Et Cosmwhim. Acta* **1986**, *50*, 693–709. [CrossRef]
9. Cai, Y.; Liu, D.; Yao, Y.; Li, J.; Qiu, Y. Geological controls on prediction of coalbed methane of No. 3 coal seam in Southern Qinshui Basin, North China. *Int. J. Coal Geol.* **2011**, *88*, 101–112. [CrossRef]
10. Chen, Y.; Tang, D.; Xu, H.; Li, Y.; Meng, Y. Structural controls on coalbed methane accumulation and high production models in the eastern margin of Ordos Basin, China. *J. Nat. Gas Sci. Eng.* **2015**, *23*, 524–537. [CrossRef]
11. Li, Y.; Tang, D.; Xu, H.; Elsworth, D.; Meng, Y. Geological and hydrological controls on water coproduced with coalbed methane in Liulin, eastern Ordos basin, China. *AAPG Bull.* **2015**, *99*, 207–229. [CrossRef]
12. Su, X.; Lin, X.; Liu, S.; Zhao, M.; Song, Y. Geology of coalbed methane reservoirs in the Southeast Qinshui Basin of China. *Int. J. Coal Geol.* **2005**, *62*, 197–210. [CrossRef]
13. Yao, Y.; Liu, D.; Tang, D.; Tang, S.; Che, Y.; Huang, W. Preliminary evaluation of the coalbed methane production potential and its geological controls in the Weibei Coalfield, Southeastern Ordos Basin, China. *Int. J. Coal Geol.* **2009**, *78*, 1–15. [CrossRef]

14. Fu, H.; Tang, D.; Xu, H.; Xu, T.; Chen, B.; Hu, P.; Yin, Z.; Wu, P.; He, G. Geological characteristics and CBM exploration potential evaluation A case study in the middle of the southern Junggar Basin, NW China. *J. Nat. Gas Sci. Eng.* **2016**, *30*, 57–570. [CrossRef]
15. Wang, B.; Li, J.; Zhang, Y.; Wang, H.; Liu, H.; Li, G.; Ma, J. Geological characteristics of low rank coalbed methane, China. *Pet. Explor. Dev.* **2009**, *36*, 30–34. [CrossRef]
16. Qin, Y.; Moore, T.A.; Shen, J.; Yang, Z.; Shen, Y.; Wang, G. Resources and geology of coalbed methane in China: A review. *Int. Geol. Rev.* **2017**, *60*, 777–812. [CrossRef]
17. Chen, Y.; Ma, Z.; Ma, D.; Zhang, Z.; Li, W.; Yang, F.; Ji, Y.; Peng, T.; Meng, Y. Characteristics of the Coal Fines Produced from Low-Rank Coal Reservoirs and Their Wettability and Settleability in the Binchang Area, South Ordos Basin, China. *Geofluids* **2021**, *2021*, 5560634. [CrossRef]
18. Gao, Z.; Ma, D.; Chen, Y.; Zheng, C.; Teng, J. Study for the Effect of Temperature on Methane Desorption Based on Thermodynamics and Kinetics. *ACS Omega* **2021**, *6*, 702–714. [CrossRef]
19. Zheng, C.; Ma, D.; Chen, Y.; Gao, Z.; Teng, J. Pore structure of different macroscopically distinguished components within low-rank coals and its methane desorption characteristics. *Fuel* **2021**, *293*, 120465. [CrossRef]
20. Yun, J.; Xu, F.; Liu, L.; Zhong, N.; Wu, X. New progress and future prospects of CBM exploration and development in China. *Int. J. Min. Sci. Technol.* **2012**, *22*, 363–369. [CrossRef]
21. Wang, X.; Cheng, Y.; Zhang, D.; Liu, Z.; Wang, Z.; Jiang, Z. Influence of tectonic evolution on pore structure and fractal characteristics of coal by low pressure gas adsorption. *J. Nat. Gas Sci. Eng.* **2021**, *87*, 103788. [CrossRef]
22. Yan, T.; Yao, Y.; Liu, D. Critical tectonic events and their geological controls on gas generation, migration, and accumulation in the Weibei coalbed methane field, southeast Ordos basin. *J. Nat. Gas Sci. Eng.* **2015**, *27*, 1367–1380. [CrossRef]
23. Li, Y.; Zhang, C.; Tang, D.; Gan, Q.; Niu, X.; Wang, K.; Shen, R. Coal pore size distributions controlled by the coalification process: An experimental study of coals from the Junggar, Ordos and Qinshui basins in China. *Fuel* **2017**, *206*, 352–363. [CrossRef]
24. Tang, S.; Tang, D.; Tang, J.; Tao, S.; Xu, H.; Geng, Y. Controlling factors of coalbed methane well productivity of multiple superposed coalbed methane systems: A case study on the Songhe mine field, Guizhou, China. *Energy Explor. Exploit.* **2017**, *35*, 665–684. [CrossRef]
25. Zhu, H.; Liu, P.; Chen, P.; Kang, J. Analysis of coalbed methane occurrence in Shuicheng Coalfield, southwestern China. *J. Nat. Gas Sci. Eng.* **2017**, *47*, 140–153. [CrossRef]
26. Lv, Y.; Tang, D.; Xu, H.; Luo, H. Production characteristics and the key factors in high-rank coalbed methane fields: A case study on the Fanzhuang Block, Southern Qinshui Basin, China. *Int. J. Coal Geol.* **2012**, *96–97*, 93–108. [CrossRef]
27. Xing, L.R.; Yao, Y.B.; Liu, D.M.; Liu, J.G.; Zhou, L.L.; Li, H.P. Geological Characteristics of Coalbed Methane Reservoir in Southern Shizhuang Block, Southeastern Qinshui Basin. *Appl. Mech. Mater.* **2013**, *295–298*, 3209–3212. [CrossRef]
28. Wang, H.; Yao, Y.; Liu, D.; Pan, Z.; Yang, Y.; Cai, Y. Fault-sealing capability and its impact on coalbed methane distribution in the Zhengzhuang field, southern Qinshui Basin, North China. *J. Nat. Gas Sci. Eng.* **2016**, *28*, 613–625. [CrossRef]
29. Du, Z.; Zhang, X.; Huang, Q.; Zhang, S.; Wang, C. The gas content distribution of coal reservoir at the Changzhi block, south-central Qinshui Basin, North China: Influences of geologic structure and hydrogeology. *Energy Explor. Exploit.* **2018**, *37*, 144–165. [CrossRef]
30. Wang, B.; Sun, F.; Tang, D.; Zhao, Y.; Song, Z.; Tao, Y. Hydrological control rule on coalbed methane enrichment and high yield in FZ Block of Qinshui Basin. *Fuel* **2015**, *140*, 568–577. [CrossRef]
31. Cao, L.; Yao, Y.; Cui, C.; Sun, Q. Characteristics of in-situ stress and its controls on coalbed methane development in the southeastern Qinshui Basin, North China. *Energy Geosci.* **2020**, *1*, 69–80. [CrossRef]
32. Lin, Y.; Qin, Y.; Ma, D.; Zhao, J. Experimental Research on Dynamic Variation of Permeability and Porosity of Low-Rank Inert-Rich Coal Under Stresses. *ACS Omega* **2020**, *5*, 28124–28135. [CrossRef] [PubMed]
33. Zhao, J.; Tang, D.; Xu, H.; Li, Y.; Tao, S.; Lin, W.; Liu, Z. Characteristic of In Situ Stress and Its Control on the Coalbed Methane Reservoir Permeability in the Eastern Margin of the Ordos Basin, China. *Rock Mech. Rock Eng.* **2016**, *49*, 3307–3322. [CrossRef]
34. Tao, S.; Tang, D.; Xu, H.; Gao, L.; Fang, Y. Factors controlling high-yield coalbed methane vertical wells in the Fanzhuang Block, Southern Qinshui Basin. *Int. J. Coal Geol.* **2014**, *134–135*, 38–45. [CrossRef]
35. Xu, H.; Tang, D.; Zhao, J.; Tao, S.; Li, S.; Fang, Y. Geologic controls of the production of coalbed methane in the Hancheng area, southeastern Ordos Basin. *J. Nat. Gas Sci. Eng.* **2015**, *26*, 156–162. [CrossRef]
36. Guo, C.; Qin, Y.; Wu, C.; Lu, L. Hydrogeological control and productivity modes of coalbed methane commingled production in multi-seam areas: A case study of the Bide–Santang Basin, western Guizhou, South China. *J. Pet. Sci. Eng.* **2020**, *189*, 107039. [CrossRef]
37. Ayers, W.B., Jr. Coalbed gas systems, resources, and production and a review of contrasting cases from the San Juan and Powder River Basins. *AAPG Bull.* **2002**, *86*, 1853–1890.
38. Bustin, R.M.; Clarkson, C.R. Geological controls on coalbed methane reservoir capacity and gas content. *Int. J. Coal Geol.* **1998**, *38*, 3–26. [CrossRef]
39. Zhao, J.; Tang, D.; Xu, H.; Lv, Y.; Tao, S. High production indexes and the key factors in coalbed methane production: A case in the Hancheng block, southeastern Ordos Basin, China. *J. Pet. Sci. Eng.* **2015**, *130*, 55–67. [CrossRef]
40. Wang, G.; Qin, Y.; Xie, Y.; Shen, J.; Zhao, L.; Huang, B.; Zhao, W. Coalbed methane system potential evaluation and favourable area prediction of Gujiao blocks, Xishan coalfield, based on multi-level fuzzy mathematical analysis. *J. Pet. Sci. Eng.* **2018**, *160*, 136–151. [CrossRef]

41. Wei, Q.; Li, X.; Hu, B.; Zhang, X.; Zhang, J.; He, Y.; Zhang, Y.; Zhu, W. Reservoir characteristics and coalbed methane resource evaluation of deep-buried coals: A case study of the No.13–1 coal seam from the Panji Deep Area in Huainan Coalfield, Southern North China. *J. Pet. Sci. Eng.* **2019**, *179*, 867–884. [CrossRef]
42. Zhang, J.; Liu, D.; Cai, Y.; Yao, Y.; Ge, X. Carbon isotopic characteristics of CH4 and its significance to the gas performance of coal reservoirs in the Zhengzhuang area, Southern Qinshui Basin, North China. *J. Nat. Gas Sci. Eng.* **2018**, *58*, 135–151. [CrossRef]
43. Li, Y.; Liu, D.M.; Yao, Y.B.; Wang, X.H.; Yin, Z.W. Evaluation of Favorable Area in the Weibei Coalbed Methane Field: A Study by Using Grey Correlation Analysis. *Appl. Mech. Mater.* **2013**, *295–298*, 3342–3345. [CrossRef]
44. Wang, W.; He, M.; Wang, X.; Jiang, P.; Peng, L.; Du, Y. Analysis on main controlling factors and comprehensive evaluation of coalbed methane production capacity of Junlian Block. *Coal Sci. Technol.* **2017**, *45*, 194–200. [CrossRef]
45. Han, J. Geochemical characteristics of South China Sea based on random forest algorithm and Wushu teaching action simulation. *Arab. J. Geosci.* **2021**, *14*, 1802. [CrossRef]
46. Zhu, Q.; Hu, Q.; Du, H.; Fan, B.; Zhu, J.; Zhang, B.; Zhao, Y.; Liu, B.; Tang, J. A gas production model of vertical coalbed methane well based on random forest algorithm. *J. China Coal Soc.* **2020**, *45*, 2846–2855. [CrossRef]
47. Dong, Y.; Du, B.; Zhang, L. Target Detection Based on Random Forest Metric Learning. *IEEE J. Sel. Top. Appl. Earth Obs. Remote Sens.* **2015**, *8*, 1830–1838. [CrossRef]
48. Wang, Q.; Chen, H.; Patnaik, S. Optimization of parallel random forest algorithm based on distance weight. *J. Intell. Fuzzy Syst.* **2020**, *39*, 1951–1963. [CrossRef]
49. Daho, M.E.H.; Chikh, M.A. Combining Bootstrapping Samples, Random Subspaces and Random Forests to Build Classifiers. *J. Med. Imaging Health Inform.* **2015**, *5*, 539–544. [CrossRef]
50. Abdi, J.; Hadipoor, M.; Esmaeili-Faraj, S.H.; Vaferi, B. A modeling approach for estimating hydrogen sulfide solubility in fifteen different imidazole-based ionic liquids. *Sci. Rep.* **2022**, *12*, 4415. [CrossRef]
51. Xu, H.; Tang, D.Z.; Liu, D.M.; Tang, S.H.; Yang, F.; Chen, X.Z.; He, W.; Deng, C.M. Study on coalbed methane accumulation characteristics and favorable areas in the Binchang area, southwestern Ordos Basin, China. *Int. J. Coal Geol.* **2012**, *95*, 1–11. [CrossRef]
52. Meng, Z.; Zhang, G.; Li, G.; Liu, J. Analysis of diffusion properties of methane in low rank coal. *Coal Geol. Explor.* **2019**, *47*, 84–89. [CrossRef]
53. Chen, S.; Tao, S.; Tian, W.; Tang, D.; Zhang, B.; Liu, P. Hydrogeological control on the accumulation and production of coalbed methane in the Anze Block, southern Qinshui Basin, China. *J. Pet. Sci. Eng.* **2021**, *198*, 108138. [CrossRef]
54. Zhang, Z.; Yan, D.; Zhuang, X.; Yang, S.; Wang, G.; Li, G.; Wang, X. Hydrogeochemistry signatures of produced waters associated with coalbed methane production in the Southern Junggar Basin, NW China. *Environ. Sci. Pollut. Res. Int.* **2019**, *26*, 31956–31980. [CrossRef] [PubMed]
55. Sang, S.; Fan, B.; Qin, Y. Conditions of Sealing and Accumulation in Coal-Bed Gas. *Oil Gas Geol.* **1999**, *20*, 104–107.
56. Bao, Y.; Wang, W.; Ma, D.; Shi, Q.; Ali, A.; Lv, D.; Zhang, C. Gas Origin and Constraint of δ13C(CH_4) Distribution in the Dafosi Mine Field in the Southern Margin of the Ordos Basin, China. *Energy Fuels* **2020**, *34*, 14065–14073. [CrossRef]
57. Whiticar, M.J. Carbon and hydrogen isotope systematics of bacterial formation and oxidation of methane. *Chem. Geol.* **1999**, *161*, 291–314. [CrossRef]
58. Wang, S. Ordos basin tectonic evolution and structural control of coal. *Geol. Bull. China* **2011**, *30*, 544–552.
59. Guo, G. Comprehensive evaluation study on favorable area of coalbed methane reservoir in southern Shizhuang Block. *Coal Sci. Technol.* **2019**, *49*, 200–206. [CrossRef]
60. Zou, Z.; Liu, D.; Cai, Y.; Wang, Y.; Li, J. Geological Factors and Reservoir Properties Affecting the Gas Content of Coal Seams in the Gujiao Area, Northwest Qinshui Basin, China. *Energies* **2018**, *11*, 1044. [CrossRef]